Journal of Cluster Science (2024) 35:1481–1491
https://doi.org/10.1007/s10876-024-02604-1

ORIGINAL PAPER

Effect of Silver-Graphene Oxide-Cobalt Oxide Nanocomposite on Cytotoxic Levels in MRC-5 and HepG2 Cell Lines and Molecular Docking Studies

Rahsan Ilikci-Sagkan[1] · Erman Salih Istifli[2] · Recep Liman[3] · Keziban Atacan[4] · Salih Zeki Bas[5] · Mustafa Ozmen[5]

Received: 1 March 2024 / Accepted: 12 March 2024 / Published online: 6 April 2024

Abstract
The cytotoxic properties of cobalt oxide (Co_3O_4) nanoparticles (NPs), in addition to graphene oxide (GO)-Co_3O_4 and silver (Ag)-GO-Co_3O_4 nanocomposites (NCs), were evaluated against both human healthy lung fibroblast (MRC-5) and hepatocellular carcinoma (HepG2) cell lines utilizing the XTT assay. The investigation revealed that synthesized Co_3O_4 NPs and NCs (GO-Co_3O_4 and Ag-GO-Co_3O_4) elicited significant cytotoxic responses in MRC-5 and HepG2 cell lines in a concentration-dependent manner. Through molecular docking analyses, it was observed that all fabricated nanomaterials exhibited DNA recognition *via* minor groove binding, with molecular affinities ranging from −4.82 to -11.66 kcal/mol. Furthermore, the docking outcomes illustrated that the angular conformations of GO-Co_3O_4 and Ag-GO-Co_3O_4 conferred 'shape-selective' characteristics as DNA minor groove binders, leading to heightened cytotoxicity, particularly in the HepG2 cell line compared to the normal MRC-5 cell line.

Keywords Cytotoxicity · Nanocomposite · Graphene · Molecular docking · Cobalt oxide · Silver

Introduction

Recent advancements in nanotechnology have enabled the integration of nanomaterials into diverse fields ranging from technology to biology and medicine. This progress hinges on the precise engineering of nanoparticles (NPs) with tailored properties. The scientific pursuit within nanoscience focuses on designing NPs with specific functionalities, miniaturizing complex structures, and ultimately, gaining deeper insights into life processes. Notably, the miniscule size of NPs endows them with unique properties that hold immense potential for modulating biological interactions [1]. Cobalt oxide nanoparticles (Co_3O_4 NPs) are categorized among metal nanoparticles and are widely utilized in both industrial (gas sensors, solar selective absorbers, lithium-ion battery anodes, pigment and dye formulation, as well as in the development of electronic thin films and magnetoresistive devices) and biomedical applications (antibacterial, antiviral, antifungal, antileishmanial, therapeutic, anticancer, and drug delivery agents) [2–8]. Graphene oxide (GO), the oxidized variant of graphene, has garnered significant attention in recent times, particularly in biomedical applications owing to its water stability, biocompatibility, large specific surface area, extensive π-conjugated structures, and abundant functional groups [9, 10]. However, some researchers have found that silver may be hybridized in other ways with other useful materials to create better composite materials. Research efforts are underway to develop GO and reduced graphene oxide (rGO) nanocomposites (NCs) or silver in conjunction with Co_3O_4 NPs for diverse

✉ Mustafa Ozmen
musozmen@gmail.com

1 School of Medicine, Department of Medical Biology, Uşak University, Uşak 64300, Turkey

2 Faculty of Science and Literature, Department of Biology, Çukurova University, Adana 01330, Turkey

3 Faculty of Engineering and Natural Sciences, Molecular Biology and Genetics Department, Uşak University, Uşak 64300, Turkey

4 Faculty of Technology, Department of Engineering Fundamental Sciences, Sakarya University of Applied Sciences, Sakarya 54050, Turkey

5 Science Faculty, Department of Chemistry, Selçuk University, Konya 42250, Turkey

biomedical applications due to their remarkable enhancements in electrical and mechanical properties. These composites exhibit improved stability, mitigate agglomeration issues, and enhance hydrophilicity in aqueous environments [11–15].

Over the past two decades, molecular docking has significantly emerged as a prominent bioinformatics method for predicting optimal binding conformations and energies in interactions between diverse receptors and ligands [16–18]. Despite the rapid proliferation of newly synthesized compounds across various domains of chemistry and industrial chemistry, there remains a lack of understanding concerning their interactions with DNA, the fundamental biomolecule accommodating cellular genetic information and crucial for life's continuation [19]. Thus, in the present study, the intermolecular interactions and binding affinities between the synthesized NPs (Co_3O_4), and NCs (GO-Co_3O_4 and Ag-GO-Co_3O_4) against the DNA molecule have been investigated using molecular docking simulations in order to understand the molecular basis of induced cytotoxicity as well as to provide a link between theoretical calculations and experiments.

In the current investigation, Co_3O_4 NPs and its graphene oxide-based NCs (GO-Co_3O_4 and Ag-GO-Co_3O_4) have been chemically synthesized. All synthesized nanomaterials were characterized using Fourier Transform Infrared Spectroscopy (FT-IR), X-ray Diffraction (XRD), and Transmission Electron Microscope (TEM) analyses. The cytotoxic impact of these nanomaterials was evaluated comparatively at physiologically relevant concentrations on both the human healthy lung fibroblast (MRC-5) cell line and hepatocellular carcinoma cell line (HepG2). Additionally, the interaction modes of synthetic nanomaterials with DNA, their affinities for DNA binding, and the ensuing intermolecular interactions were scrutinized at the molecular level employing molecular docking techniques. This analysis provided insights into the mechanistic underpinnings of experimentally-induced cytotoxicity, as well as the rationale behind utilizing these nanomaterials as potential anti-cancer agents (Scheme 1). Several nanoparticles are presently being assessed in our laboratory as part of our continuous efforts to find and comprehend the mechanisms of action of innovative and useful nanoparticles. Here, the mechanistic aspects of nanomaterials-induced cell death were reported in the MRC-5 and HepG2 cell lines.

Materials and Methods

The materials, apparatus, and synthesis of nanomaterials used in this study are presented in the Supplementary Material.

XTT Cell Cytotoxicity Assay

The MRC-5 and HepG2 cell lines were cultured in accordance with ATCC guidelines. They were cultured in Dulbecco's modified Eagle's medium (DMEM) supplemented with 0.1% streptomycin/penicillin (PS-B, Capricorn), L-Glutamine (Capricorn), and 10% fetal bovine serum. Using T75 culture flasks, the cultures were grown in a humidified incubator with a temperature control of 37 °C and 5% CO_2. Trypsin-EDTA was used for subculturing at preconfluent densities.

The standard 2,3-bis-[2 methoxy-4-nitro-5-sulfophenyl] − 2 H-tetrazolium-5-carboxanilide inner salt (XTT) assay kit was used to quantify the metabolic activity of live cells in order to determine cell proliferation. Initially, 10,000 cells per well of 96-well microplates were used to seed MRC-5 and HepG2 cells. After allowing cells to attach overnight in growth medium, the medium was changed out for new one containing indicated concentrations of Co_3O_4, GO-Co_3O_4, and Ag-GO-Co_3O_4 nanoparticles and nanocomposites (10, 25, 50, 100, 200, and 300 µg/mL). To prevent particle aggregation, suspensions underwent sonication for 10 min at 40 W prior to cell treatment. Untreated cells served as controls. In the XTT assay, cell cultures were exposed to the samples for 24 h, followed by the addition of 50 µL of XTT reagent for a further 4-hour incubation period. Metabolically active cells metabolize the XTT reagent, producing an orange formazan dye whose concentration correlates directly with cellular viability. When XTT was reduced extracellularly in untreated cells, the formazan dye product's absorbance level was determined to be 100% vitality. One-way ANOVA followed by the Duncan test was done for the significance study using a significance set at $p < 0.05$. Furthermore, the selectivity index (SI) values were computed in the manner described below to ascertain the relative efficacy of nanoparticles and nanocomposites in causing the death of cancer cells relative to the death of normal cells.

SI = IC_{50} value of healthy human lung fibroblast cells/ IC_{50} value of hepatocellular carcinoma cells.

Receptor and Ligands' Retrieval and Execution of Molecular Docking Simulations Using AutoDock Vina

In this present research, molecular scale docking calculations were employed utilizing AutoDock Vina 1.2.3 (latest version) [20]. Therefore, the binding conformations as well as the binding free energy (ΔG) values of nanomaterials obtained as a result of the interactions of cobalt oxide (Co_3O_4) nanoparticle (NP), graphene oxide—cobalt oxide (GO-Co_3O_4) nanocomposite (NC), and silver—graphene

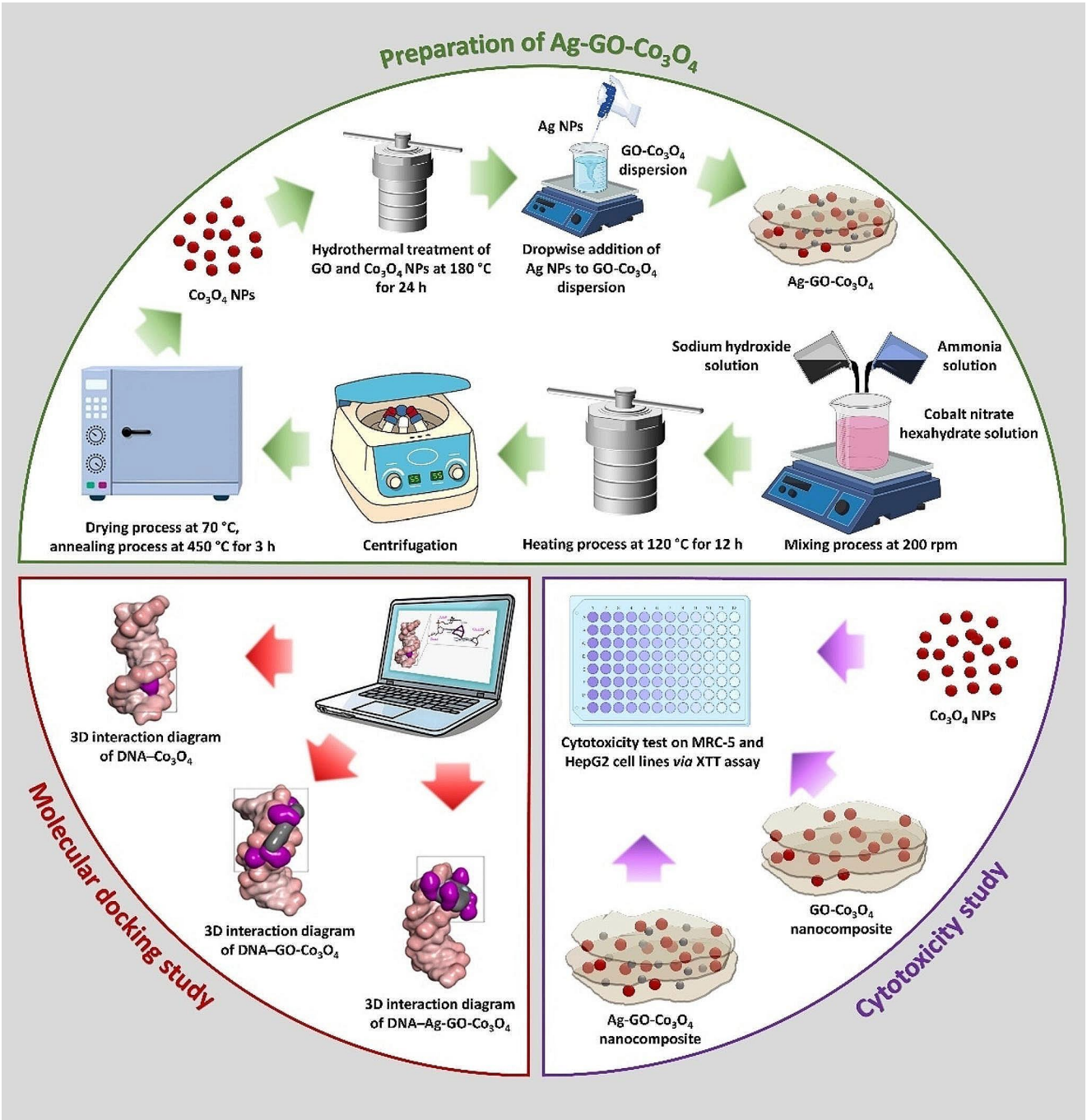

Scheme 1 Schematic illustration of nanomaterials preparation and their application in cytotoxicity and molecular docking studies

oxide—cobalt oxide (Ag-GO-Co_3O_4) NC complexes against the B-DNA dodecamer, crystal structure of a high resolution DNA conformation, were calculated. The crystallographic 12-mer B-DNA dodecamer (PDB ID: 7rqt; resolution: 1.26 Å), utilized as the receptor model in molecular docking experiments, was obtained from the Nucleic Acid Database (NDB, http://ndbserver.rutgers.edu/) in the pdb format, whereas the ligands Co_3O_4, GO-Co_3O_4, Ag-GO-Co_3O_4 were sketched in 3D using CorelDRAW Graphics Suite (version 12.0) and subsequently saved in the mol2 format. Geometry optimization of all ligands were performed using UFF (united-atom force field) in the Avogadro program [21]. Prior to commencing molecular docking simulations, initial preparation involving the setup of both target (B-DNA) and ligand structures, alongside the adjustment of parameters related to docking, was conducted utilizing AutoDock Tools 1.5.6 [22]. During the docking calculations, polar hydrogen atoms were retained on both the target

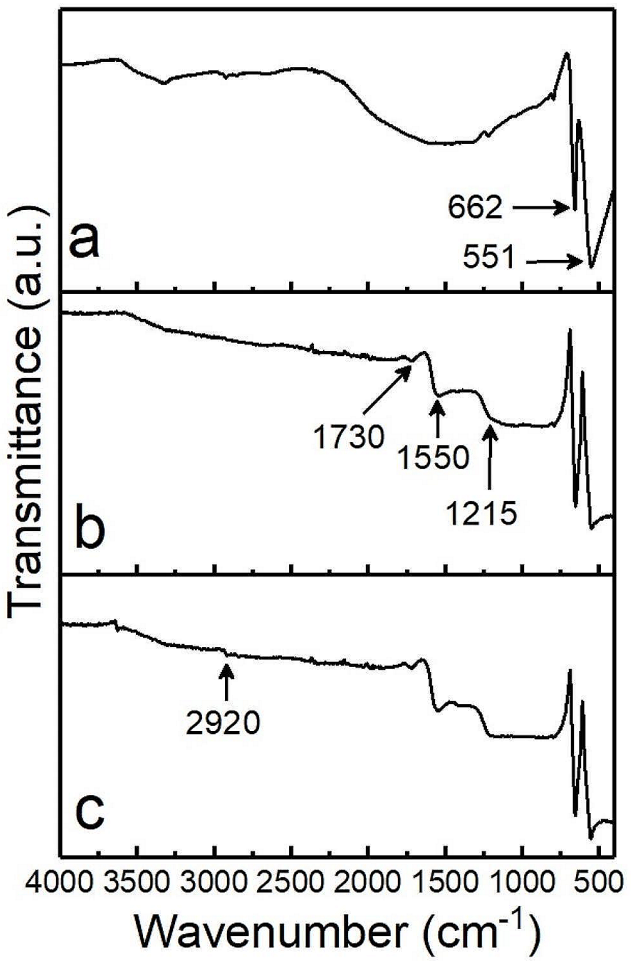

Fig. 1 FT-IR spectra of Co_3O_4 (a), GO-Co_3O_4 (b), and Ag-GO-Co_3O_4 (c)

receptor and interacting ligands, whereas non-polar hydrogen atoms were eliminated. The DNA dodecamer, receptor structure, was assigned Kollmann charges, whereas the ligands were assigned Gasteiger charges. In this docking strategy, characterized as semi-flexible (rigid receptor-flexible ligand), the rotatable bonds, if existing, within ligands were permitted to rotate freely during docking trials. This semi-flexible approach enhances precision in forecasting ligand binding orientations and strengths. The dimensions of the grid box, spanning all the major and minor grooves of the target receptor, were constructed as 62 × 72 × 116 Å points (x = 15.51; y = 20.95; z = 9.74), with a grid resolution set at 0.375 Å. Subsequently, using the AutoDock Tools 1.5.6, the optimized structures of receptor and ligands were then saved in pdbqt format and submitted for docking simulations. For each ligand, we performed 20 distinct docking iterations against the target DNA, employing an *exhaustiveness* setting of '100'. Subsequently, the resultant docking configurations were sorted based on the binding free energy (ΔG; kcal/mol) assigned to each docking pose. Post-docking

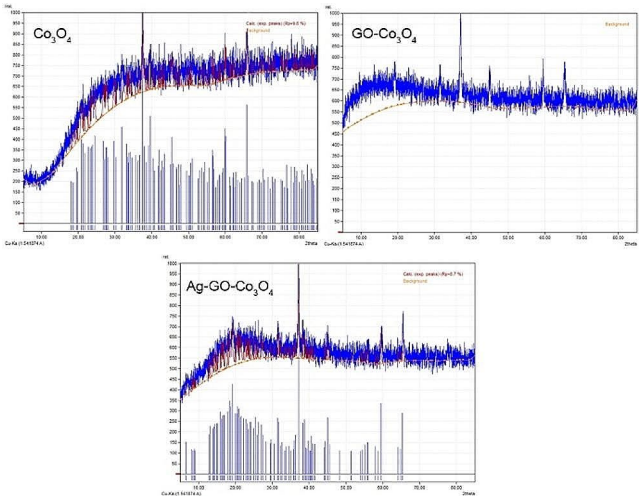

Fig. 2 XRD spectra of Co_3O_4, GO-Co_3O_4, and Ag-GO-Co_3O_4.

interactions between the DNA receptor and ligands were analyzed for the most favorable docking conformations, selected from among 20 randomly generated poses for each ligand against the DNA receptor, utilizing the DS Visualizer (version v16) software.

Results and Discussion

Characterization of Nanomaterials

The FT-IR spectrum of Co_3O_4 displays two absorption peaks at 662 cm^{-1} and 551 cm^{-1}, which correspond to the Co-O stretching vibrations (Fig. 1a) [23, 24]. In the case of GO (Fig. 1b), the characteristic peak observed at 1730 cm^{-1} can be attributed to the C = O stretching vibration of carboxylic acid. Additionally, the bands seen at 1215 cm^{-1} and 1050 cm^{-1} are associated with the -C-H and C-O stretching vibrations, respectively. Furthermore, the peak observed at approximately 3400 cm^{-1} is due to -OH tensile vibration, as GO still contains a small amount of residual water molecules [25]. In the FTIR spectrum of Ag-GO-Co_3O_4 nanocomposite (Fig. 1c), slight shifts in the peaks and decrease in peak intensities are thought to be due to the reduction of Ag nanoparticles [26].

Figure 2 shows the raw XRD patterns of the as-prepared Co_3O_4, GO-Co_3O_4, and Ag-GO-Co_3O_4 nanomaterials. As seen in the XRD pattern of Co_3O_4 nanoparticles, there are three strong intense diffraction lines at around 2θ of 38° (311), 60° (511), and 66° (440), respectively [27]. The diffraction peak of GO shifted to approximately 32° in Fig. 2. This indicates a decrease in the sp^2 carbon fraction [28]. In the composite of Ag-GO-Co_3O_4 nanomaterial, the peaks observed at around 32°, 45°, 47°, and 56° corresponded to

the (122), (200), (231), and (142) crystallographic planes of the Ag nanoparticles phase [29].

Figure 3 delineates TEM (a, b, c) and HRTEM (d, e, f) photographs of Ag-GO-Co_3O_4. The Ag nanoparticles were observed on the Co_3O_4 nanoparticles and graphene surfaces (Fig. 3a,b) [30, 31]. As shown in Fig. 3d, the lattice plane spacing of 0.28 nm matches well with (220) of cubic Co_3O_4 [32]. As illustrated in Fig. 3e, the lattice spacing of 0.24 and 0.24 nm correspond to the (200) and (311) crystal planes of Ag and the Co_3O_4, respectively [31, 33]. In addition, the d-spacing near the edge is about 0.46 nm and 0.23 nm, which corresponds to the (111) lattice planes of Co_3O_4 and the (001) plane of GO in Fig. 3f [34, 35]. Figure 3g indicates EDX spectrum of Ag-GO-Co_3O_4. In addition, the EDX result represents the existence of elements Ag, Co, O and C. Moreover, the EDX spectra and TEM photos of Co_3O_4 and GO-Co_3O_4 were illustrated in Figure S1 and Figure S2, respectively (Supplementary Information).

Cytotoxicity Assay on MRC-5 and HepG2 Cells

Three types of nanomaterials (Co_3O_4 NP, GO-Co_3O_4 and Ag-GO-Co_3O_4 NCs) were obtained successively based on cobalt using solvothermal method. The cytotoxic activity

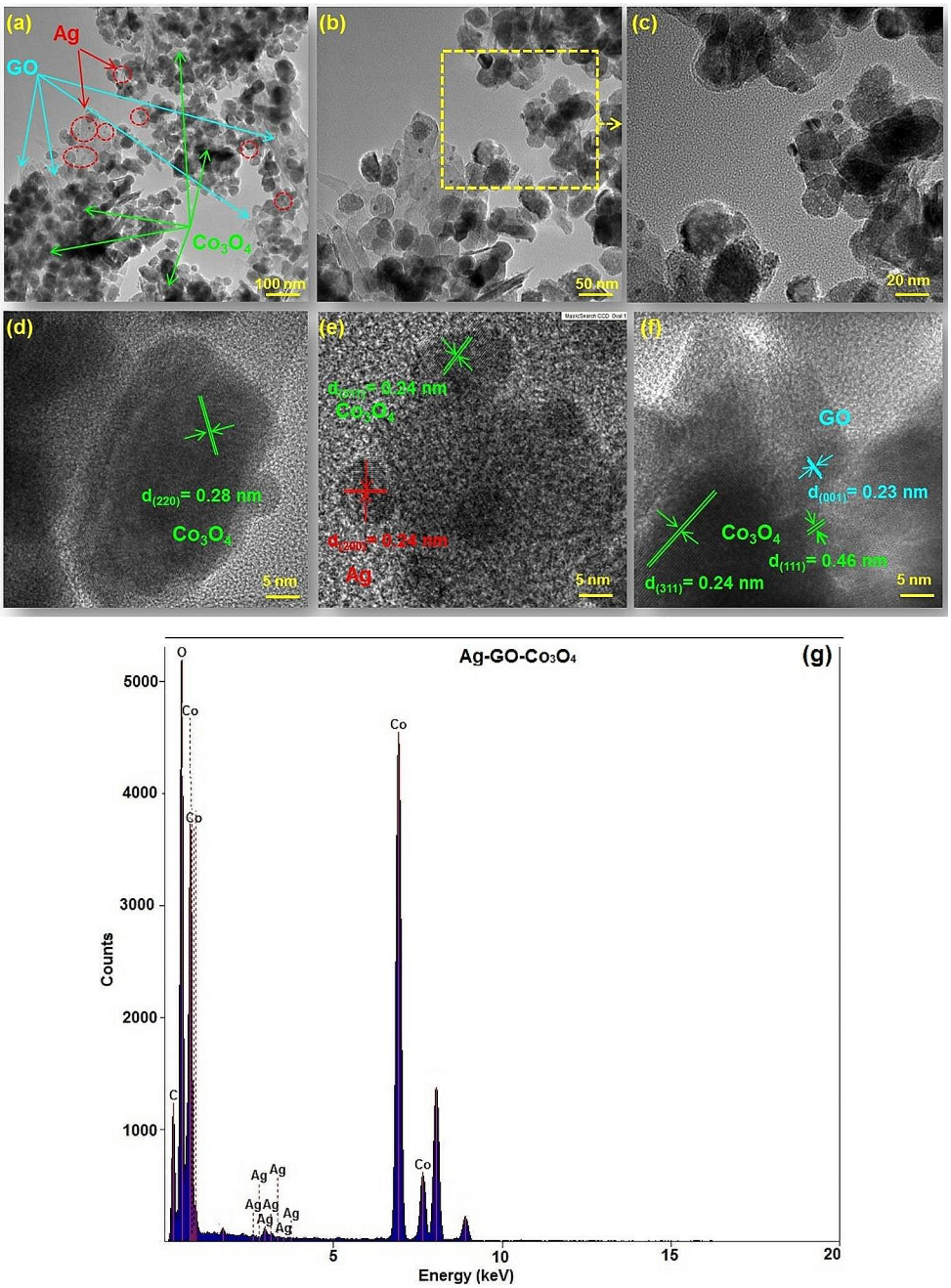

Fig. 3 TEM (a, b, c) and HRTEM (d, e, f) photographs and EDX (g) profile of Ag-GO-Co_3O_4.

of the nanomaterials including Co_3O_4, GO-Co_3O_4, and Ag-GO-Co_3O_4 was evaluated *in vitro* using two human cell lines (MRC-5 and HepG2). Using the XTT assay, the cytotoxic effect of Co_3O_4 NP, GO-Co_3O_4, and Ag-GO-Co_3O_4 NCs was assessed by monitoring the metabolic activity in living cells. We suspected that Ag-GO-Co_3O_4 NC is more cytotoxic on HepG2 cell line compared to MRC-5 lung fibroblast cell line after 24-h treatment. The results showed that all nanomaterials inhibited cell proliferation in a dose dependent manner above 10 µM (Fig. 4). The results also demonstrated that, after a 24-hour treatment, Ag-GO-Co_3O_4 NC is more cytotoxic on HepG2 cell line compared to MRC-5 lung fibroblast cell line. The induced cytotoxic effect on HepG2 cell line was found to be greater by GO-Co_3O_4 and Ag-GO-Co_3O_4 NCs treatments than in Co_3O_4 NP treatment alone. In the case of the Ag-GO-Co_3O_4 NC especially at high concentrations, a combined synergistic effect was found between Ag, GO and Co_3O_4, leading to the reduction of cell viability and induction of cancer cell death. Furthermore, alongside modifying cell morphology, the Ag-GO-Co_3O_4 NC may reduce cellular metabolic activity, elevates oxidative stress levels through the generation of reactive oxygen species or may induce ROS-independent mitochondrial dysfunction, which led to the reduction of energy metabolism and inhibition of proliferation [36–42, 15, 43–45]. The selective cytotoxic activity Co_3O_4, GO-Co_3O_4, and Ag-GO-Co_3O_4 in human hepatocellular carcinoma (HepG2) cells was compared using a healthy human lung fibroblast (MRC-5) cell line. The IC_{50} values of Co_3O_4 NP, GO-Co_3O_4, and Ag-GO-Co_3O_4 NCs were found to be 196.92 ± 9.64 µg/mL, 165.54 ± 1.22 µg/mL, and 157.27 ± 0.58 µg/mL in the healthy cells, respectively. Similarly, in the liver cancer cells, the IC_{50} values were found to be 196.92 ± 0.18 µg/mL, 162.38 ± 0.76 µg/mL, and 127.40 ± 1.13 µg/mL. The IC_{50} values of nanomaterials on MRC-5 cells were compared with HepG2 cells to evaluate the selectivity index (SI) values. A compound's ability to selectively inhibit proliferation in abnormal cells while avoiding harm in normal cells is shown by its SI value [46]. Among all the synthesized nanomaterials (Co_3O_4,

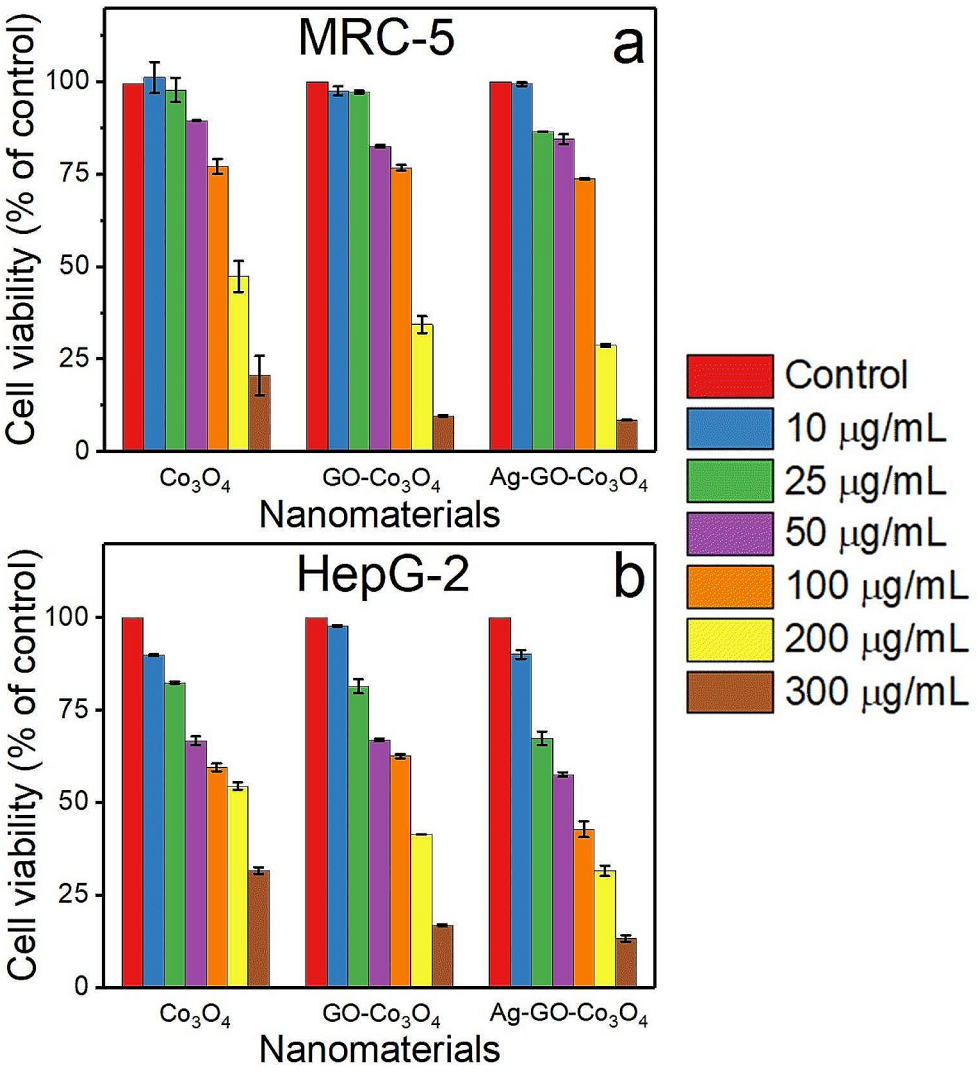

Fig. 4 Effect of nanomaterials on the cell proliferation of MRC-5 (a) and HepG2 (b) cell lines determined by XTT assay after 24-h incubation

Table 1 IC_{50} and SI values of nanomaterials on human normal lung fibroblast and hepatocellular carcinoma cell lines

Nanomaterials	MRC-5 IC_{50} (µg/mL)	HepG2 IC_{50} (µg/mL)	SI
Co_3O_4	196.92 ± 9.64a*	196.92 ± 0.18a	1.00
GO-Co_3O_4	165.54 ± 1.22b	162.38 ± 0.76bc	1.02
Ag-GO-Co_3O_4	157.27 ± 0.58c	127.40 ± 1.13d	1.23

GO-Co_3O_4, and Ag-GO-Co_3O_4) tested, Ag-GO-Co_3O_4 NC had an SI value (1.23) which was higher than other tested nanomaterials for the HepG2 cell line (Table 1). We found that based on the calculated SI (> 1.00), Ag-GO-Co_3O_4 NC could show anti-cancer activity against the HepG2 cells versus healthy MRC-5 cells; thus, according to the IC_{50} values, Ag-GO-Co_3O_4 NC presumed to be non-toxic and bioactive.

* Different letters$^{(a-d)}$ on table are statistically significant at $p \leq 0.05$. Data were depicted as the mean ± standard deviation (SD), with a sample size of $n = 3$. SI is equal to the IC_{50} value of hepatocellular carcinoma cells divided by the IC_{50} value of normal human lung fibroblasts.

Interactions of Synthesized Nanomaterials against DNA

Table 2; Fig. 5A, B present the target (DNA) affinity, binding conformation, and molecular contacts between the Co_3O_4 nanoparticle (NP) and DNA, as revealed by the docking simulation. Co_3O_4 exhibited a preferred binding pose wherein it interacted with the minor groove of DNA. This binding mode involved the formation of multiple hydrogen bonds with G4, A5, and G22, along with Van der Waals contacts with A6, C21, and C23 (Table 2). The binding affinity (ΔG; kcal/mol) of Co_3O_4 NP against the DNA was found energetically favorable ($\Delta G_{best} = -4.82$; $\Delta G_{average} = -4.39$) (Table 2).

ΔG_{best}: Binding free energy of the most favorable pose (binding mode).

$\Delta G_{average}$: The average of the binding free energy values obtained as a result of 20 independent docking runs.

GO-Co_3O_4: Graphene oxide—cobalt oxide NC.

Ag-GO-Co_3O_4: Silver—graphene oxide—cobalt oxide NC.

Table 2; Fig. 5C, D depict the target (DNA) affinity, binding conformation, and molecular contacts between the GO-Co_3O_4 nanocomposite (NC) and DNA. It is evident that GO-Co_3O_4 fits snugly within the minor groove of the DNA fragment in its optimal binding conformation. This conformation shows numerous hydrogen bond interactions with A6, T7, T20, G22, and C23, along with a limited number of Van der Waals contacts with G4, T19, and G24, electrostatic interactions with C21 and G22, and a hydrophobic pi-alkyl interaction with A5 (Table 2). The computed binding energy of GO-Co_3O_4 NC with the DNA fragment demonstrates a thermodynamically highly favorable state ($\Delta G_{best} = -11.66$; $\Delta G_{average} = -11.29$) (Table 2).

Table 2; Fig. 5E, F provide insights into the target (DNA) affinity, binding conformation, and molecular contacts of the Ag-GO-Co_3O_4 nanocomposite (NC) with DNA. Similar to the GO-Co_3O_4 NC, the Ag-GO-Co_3O_4 NC fits snugly within the minor groove of the DNA fragment, predominantly positioning its Co_3O_4 components upwards (Fig. 5E). It forms hydrogen bonding with G4, numerous Van der Waals contacts with G2, C3, G22, and C23, electrostatic interactions with A5 and A6, and ultimately, a metal-acceptor interaction with G24 (Table 2). Despite being slightly lower compared to the GO-Co_3O_4 NC, the interaction energy derived from the docking of Ag-GO-Co_3O_4 NC with DNA remains thermodynamically highly advantageous ($\Delta G_{best} = -11.51$; $\Delta G_{average} = -9.51$) (Table 2).

It can be inferred that there exists a certain degree of correlation between the calculated IC_{50} values and docking scores for Co_3O_4 NP, GO-Co_3O_4 NC, and Ag-GO-Co_3O_4 NC in the MRC-5 cell line. As the molecular weight of synthetic ligands increases (Table 3), there is an observed escalation in the cytotoxic response manifested in MRC-5 healthy cells, attributed to their DNA-binding strengths (Table 2), supported by the decrease in IC_{50} values (Table 1).

In the HepG2 cell line, there is generally observed a lower correlation between the docking scores and IC_{50}

Table 2 The molecular docking analyses provided data on the binding free energies (ΔG) and the interactions between the DNA nucleotides and cobalt oxide (Co_3O_4) nanoparticles (NPs), as well as the GO-Co_3O_4 and Ag-GO-Co_3O_4 nanocomposites (NCs).

Compound	Receptor	ΔG_{best} (kcal/mol)	$\Delta G_{average}$ (kcal/mol)	Binding mode	H-bonds (classic and carbon-hydrogen)	Van der Waals	Electrostatic	Hydrophobic (pi-alkyl)	Other (metal-acceptor)
Co_3O_4	B-DNA	-4.82	-4.39	Minor groove	G4, A5, G22	A6, C21, C23	-	-	-
GO-Co_3O_4	B-DNA	-11.66	-11.29	Minor groove	A6, T7, T20, G22, C23	G4, T19, G24	C21, G22	A5	-
Ag-GO-Co_3O_4	B-DNA	-11.51	-9.51	Minor groove	G4	G2, C3, G22, C23	A5, A6	-	G24

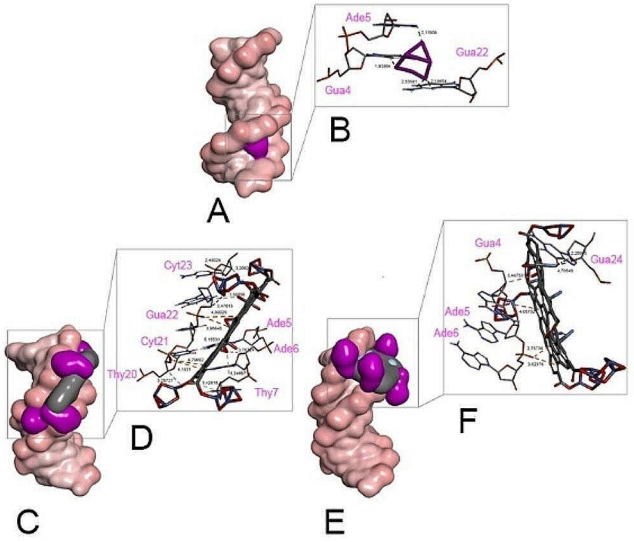

Fig. 5 The graphical representations in Figs. A, C, and E illustrate the molecular surface and binding conformations of the top-ranked docking complexes formed by various synthetic nanomaterials in complex with double-stranded (ds) DNA, accompanied by three-dimensional (3D) nucleotide interaction diagrams for each synthetic compound with DNA, as shown in B, D, and F. Specifically, Figs. (A, B) depict the binding mode and 3D nucleotide interaction diagram of Co_3O_4 with DNA; (C, D) exhibit the binding mode and 3D nucleotide interaction diagram of GO-Co_3O_4 NC with DNA; and (E, F) present the binding mode and 3D nucleotide interaction diagram of the Ag-GO-Co_3O_4 nanocomposite with DNA. It is noteworthy that all synthetic nanomaterials snugly accommodate within the minor grooves of DNA, indicative of their shape-selective affinity towards DNA. Visualizations were generated using the DS Studio v16 software package

Table 3 Calculated lowest energies of nanoparticles and nanocomposites based on the Universal Force Field (UFF).

Ligand	Molecular weight (g/mol)	Intramolecular energy (kJ/mol)
Co_3O_4	240.799	846.1
GO-Co_3O_4	2090.16	8547
Ag-GO-Co_3O_4	2627.49	12747.4

Co_3O_4: Cobalt oxide nanoparticle

GO-Co_3O_4: Graphene oxide—cobalt oxide nanocomposite

Ag-GO-Co_3O_4: Silver—graphene oxide—cobalt oxide nanocomposite

values compared to the healthy (MRC-5) cell line (Tables 1 and 2). However, despite the Ag-GO-Co_3O_4 ligand exhibiting slightly weaker DNA-binding energy compared to GO-Co_3O_4 (Table 2), this data does not correlate with the IC_{50} value of the Ag-GO-Co_3O_4 NC and the cytotoxic effect of Ag-GO-Co_3O_4 NC in the HepG2 cell line was found greater than that of GO-Co_3O_4 (Table 1; Fig. 4b). Moreover, an association between molecular energy and cellular toxicity levels (particularly in HepG2 cells) could be anticipated. The calculated intramolecular energy ranking based on molecular configuration has been found as: Ag-GO-Co_3O_4 > GO-Co_3O_4 > Co_3O_4 (Table 3). Hence, the nanocomposite Ag-GO-Co_3O_4, characterized by the lowest stability, demonstrates notably increased cytotoxic effects, particularly on the HepG2 cancer cell line. This could be expected since chemically unstable and bulky molecules often induce toxicity by binding to biological macromolecules, including DNA and proteins [47].

In the MRC-5 cell line, both the NP and the two NCs exhibit toxicity, starting from the higher concentrations of 200 and 300 µg/mL. However, promisingly, in the HepG2 cell line, the NP and two NCs exert toxicity starting from concentrations as low as 50 µg/mL, escalating at concentrations of 100, 200, and 300 µg/mL (Fig. 4a, b). Hence, it can be inferred that the toxic effects of Co_3O_4, GO-Co_3O_4, and Ag-GO-Co_3O_4 on the HepG2 cell line could be differential and more potent. It is essential to highlight that owing to their rigid planar structures and continuous occupation of the minor grooves of DNA, the interaction between these engineered synthetic nanomaterials and DNA likely follows a *lock-and-key* mechanism. This mechanism primarily relies on three fundamental elements: hydrogen bonding, Van der Waals contacts, and electrostatic interactions, which align with our findings from docking interaction results (Table 2) [48, 49].

Conclusion

In this study, it was observed that cell death increased in a dose-dependent manner across two examined cell lines (except 10 µg/mL of Co_3O_4 in MRC-5 cell line). The toxicity of Ag-GO-Co_3O_4 nanocomposite especially at high concentrations tested was observed to be greater compared to other nanomaterials. In molecular docking experiments, it has been observed that synthetic nanoparticles (Co_3O_4) and nanocomposites (GO-Co_3O_4 and Ag-GO-Co_3O_4) energetically form highly favorable complexes with the 12-nucleotide high resolution B-DNA dodecamer through minor groove recognition mode, and the DNA affinities, particularly for GO-Co_3O_4 and Ag-GO-Co_3O_4, were found to be sufficiently strong to induce a high level of toxicity. Furthermore, when experimental results are combined with docking interaction analysis, Ag-GO-Co_3O_4 may possess the intrinsic capability to elicit higher toxicity in HepG2 cancer cell lines. Nevertheless, it is imperative to reinforce these findings with additional *wet-lab* studies to comprehensively elucidate the mechanisms underlying the safe utilization and management of these synthetic nanomaterials across various applications.

Supplementary Information The online version contains supplementary material available at https://doi.org/10.1007/s10876-

024-02604-1.

Acknowledgements We express our gratitude to the EngSurf-Twin project, funded by the EU Horizon 2020 program (Grant Number 952289).

Author Contributions RIS: conceptualization, methodology, writing—original draft preparation. ESI: conceptualization, methodology, data curation, writing—original draft preparation RL: methodology, writing—original draft preparation KA, SZB, and MO: conceptualization, investigation, writing—original draft preparation, reviewing and editing.

Funding Open access funding provided by the Scientific and Technological Research Council of Türkiye (TÜBİTAK).

Data Availability No datasets were generated or analysed during the current study.

Declarations

Ethical Approval Not applicable.

Consent to Participate The authors declare our consent to participate.

Consent for publication The authors declare our consent for publication upon acceptance.

Competing Interests The authors declare no competing interests.

Conflict of interest The authors declare that they have no conflict of interest. No potential conflict of interest was reported by the authors.

References

1. Nouri, M., Esfahanizadeh, N., Shahpar, M. G., Attar, F., Sartipnia, N., Akhtari, K., et al. (2018). Cobalt oxide nanoparticles mediate tau denaturation and cytotoxicity against PC-12 cell line. International Journal of Biological Macromolecules, *118*, 1763–1772, doi:https://doi.org/10.1016/j.ijbiomac.2018.07.024.
2. Anuradha, C. T., & Raji, P. (2022). Facile-synthesis and characterization of cobalt oxide (Co_3O_4) nanoparticles by using Arishta leaves assisted biological molecules and its antibacterial and antifungal activities. Journal of Molecular Structure, *1262*, 133065, doi:https://doi.org/10.1016/j.molstruc.2022.133065.
3. Bhalla, V., & Tyagi, H. (2017). Solar energy harvesting by cobalt oxide nanoparticles, a nanofluid absorption based system. Sustainable Energy Technologies and Assessments, *24*, 45–54, doi:https://doi.org/10.1016/j.seta.2017.01.011.
4. Huang, X., Cai, H., Zhou, H., Li, T., Jin, H., Evans, C. E., et al. (2021). Cobalt oxide nanoparticle-synergized protein degradation and phototherapy for enhanced anticancer therapeutics. Acta Biomaterialia, *121*, 605–620, doi:https://doi.org/10.1016/j.actbio.2020.11.036.
5. Iqbal, J., Abbasi, B. A., Batool, R., Khalil, A. T., Hameed, S., Kanwal, S., et al. (2019). Biogenic synthesis of green and cost effective cobalt oxide nanoparticles using Geranium wallichianum leaves extract and evaluation of in vitro antioxidant, antimicrobial, cytotoxic and enzyme inhibition properties. Materials Research Express, *6*(11), 115407, doi:https://doi.org/10.1088/2053-1591/ab4f04.
6. Li, W., Jung, H., Hoa, N. D., Kim, D., Hong, S.-K., & Kim, H. (2010). Nanocomposite of cobalt oxide nanocrystals and single-walled carbon nanotubes for a gas sensor application. Sensors and Actuators B: Chemical, *150*(1), 160–166, doi:https://doi.org/10.1016/j.snb.2010.07.023.
7. Shanmuganathan, R., Sathiyavimal, S., Hoang Le, Q., M. Al-Ansari, M., A. Al-Humaid, L., Jhanani, G. K., et al. (2023). Green synthesized Cobalt oxide nanoparticles using Curcuma longa for anti-oxidant, antimicrobial, dye degradation and anti-cancer property. Environmental Research, *236*, 116747, doi:https://doi.org/10.1016/j.envres.2023.116747.
8. Wang, D., Yu, Y., He, H., Wang, J., Zhou, W., & Abruña, H. D. (2015). Template-Free Synthesis of Hollow-Structured Co_3O_4 Nanoparticles as High-Performance Anodes for Lithium-Ion Batteries. ACS Nano, *9*(2), 1775–1781, doi:https://doi.org/10.1021/nn506624g.
9. Chung, C., Kim, Y.-K., Shin, D., Ryoo, S.-R., Hong, B. H., & Min, D.-H. (2013). Biomedical Applications of Graphene and Graphene Oxide. Accounts of Chemical Research, *46*(10), 2211–2224, doi:https://doi.org/10.1021/ar300159f.
10. Singh, D. P., Herrera, C. E., Singh, B., Singh, S., Singh, R. K., & Kumar, R. (2018). Graphene oxide: An efficient material and recent approach for biotechnological and biomedical applications. Materials Science and Engineering: C, *86*, 173–197, doi:https://doi.org/10.1016/j.msec.2018.01.004.
11. Alsharaeh, E., Mussa, Y., Ahmed, F., Aldawsari, Y., Al-Hindawi, M., & Sing, G. K. (2016). Novel route for the preparation of cobalt oxide nanoparticles/reduced graphene oxide nanocomposites and their antibacterial activities. *Ceramics International, 42*(2, Part B), 3407–3410, doi:https://doi.org/10.1016/j.ceramint.2015.10.135.
12. Gholivand, K., Sabaghian, M., Babaei, A., Eshaghi Malekshah, R., Sadeghi-Mohammadi, S., & Naderi-Manesh, H. (2023). Phytic acid-modified graphene/cobalt oxide nanocomposites: synthesis, characterization, theoretical studies, antiproliferative properties, and catalytic activities. New Journal of Chemistry, *47*(17), 8363–8380, doi:https://doi.org/10.1039/D3NJ00091E.
13. Hatamie, S., Ahadian, M. M., Soufi Zomorod, M., Torabi, S., Babaie, A., Hosseinzadeh, S., et al. (2019). Antibacterial properties of nanoporous graphene oxide/cobalt metal organic framework. Materials Science and Engineering: C, *104*, 109862, doi:https://doi.org/10.1016/j.msec.2019.109862.
14. Kiani, M., Rabiee, N., Bagherzadeh, M., Ghadiri, A. M., Fatahi, Y., Dinarvand, R., et al. (2021). Improved green biosynthesis of chitosan decorated Ag- and Co_3O_4-nanoparticles: A relationship between surface morphology, photocatalytic and biomedical applications. Nanomedicine: Nanotechnology, Biology and Medicine, *32*, 102331, doi:https://doi.org/10.1016/j.nano.2020.102331.
15. Mishra, A., Singh, A., Kushwaha, H. R., & Mishra, A. (2022). Cytotoxic effect of cobalt oxide–graphene oxide nanocomposites on melanoma cell line. Journal of Experimental Nanoscience,

17(1), 509–521, doi:https://doi.org/10.1080/17458080.2022.2115483.
16. Fan, J., Fu, A., & Zhang, L. (2019). Progress in molecular docking. Quantitative Biology, *7*(2), 83–89, doi:https://doi.org/10.1007/s40484-019-0172-y.
17. Ikram, M., Rasheed, F., Haider, A., Naz, S., Ul-Hamid, A., Shahzadi, A., et al. (2022). Photocatalytic and antibacterial activity of graphene oxide/cellulose-doped TiO_2 quantum dots: in silico molecular docking studies. Nanoscale Advances, *4*(18), 3764–3776, doi:https://doi.org/10.1039/D2NA00383J.
18. Mehmandoust, M., Pourhakkak, P., Tiris, G., Karimi-Maleh, H., & Erk, N. (2022). A reusable and sensitive electrochemical sensor for determination of idarubicin in environmental and biological samples based on $NiFe_2O_4$ nanospheres anchored N-doped graphene quantum dots composite; an electrochemical and molecular docking investigation. Environmental Research, *212*, 113264, doi:https://doi.org/10.1016/j.envres.2022.113264.
19. Ricci, C. G., & Netz, P. A. (2009). Docking Studies on DNA-Ligand Interactions: Building and Application of a Protocol To Identify the Binding Mode. Journal of Chemical Information and Modeling, *49*(8), 1925–1935, doi:https://doi.org/10.1021/ci9001537.
20. Trott, O., & Olson, A. J. (2010). AutoDock Vina: Improving the speed and accuracy of docking with a new scoring function, efficient optimization, and multithreading. Journal of Computational Chemistry, *31*(2), 455–461, doi:https://doi.org/10.1002/jcc.21334.
21. Hanwell, M. D., Curtis, D. E., Lonie, D. C., Vandermeersch, T., Zurek, E., & Hutchison, G. R. (2012). Avogadro: an advanced semantic chemical editor, visualization, and analysis platform. Journal of Cheminformatics, *4*(1), 17, doi:https://doi.org/10.1186/1758-2946-4-17.
22. Sanner, M. F. (1999). Python: a programming language for software integration and development. Journal of molecular graphics & modelling, *17*(1), 57–61.
23. Turkkan, G., Bas, S. Z., Atacan, K., & Ozmen, M. (2022). An electrochemical sensor based on a Co_3O_4–ERGO nanocomposite modified screen-printed electrode for detection of uric acid in artificial saliva. Analytical Methods, *14*(1), 67–75, doi:https://doi.org/10.1039/D1AY01744F.
24. Vinodhkumar, G., Ramya, R., Potheher, I. V., Vimalan, M., & Peter, A. C. (2019). Synthesis of reduced graphene oxide/Co_3O_4 nanocomposite electrode material for sensor application. Research on Chemical Intermediates, *45*(5), 3033–3051, doi:https://doi.org/10.1007/s11164-019-03777-5.
25. Demir, N., Atacan, K., Ozmen, M., & Bas, S. Z. (2020). Design of a new electrochemical sensing system based on MoS_2–TiO_2/reduced graphene oxide nanocomposite for the detection of paracetamol. New Journal of Chemistry, *44*(27), 11759–11767, doi:https://doi.org/10.1039/D0NJ02298E.
26. Sahu, D., Sarkar, N., Mohapatra, P., & Swain, S. K. (2020). Rhodamine B associated Ag/r-GO nanocomposites as ultrasensitive fluorescent sensor for Hg^{2+}. Microchemical Journal, *154*, 104577, doi:https://doi.org/10.1016/j.microc.2019.104577.
27. Zhang, W., Lassen, K., Descorme, C., Valverde, J. L., & Giroir-Fendler, A. (2021). Effect of the precipitation pH on the characteristics and performance of Co_3O_4 catalysts in the total oxidation of toluene and propane. Applied Catalysis B: Environmental, *282*, 119566, doi:https://doi.org/10.1016/j.apcatb.2020.119566.
28. Hossain, Md. D., Zhang, Q., Cheng, T., Goddart, W. A., & Luo, Z. (2021). Graphitization of low-density amorphous carbon for electrocatalysis electrodes from ReaxFF reactive dynamics. Carbon, *183*, 940–947, doi: https://doi.org/10.1016/j.carbon.2021.07.080.
29. Kumar, A., Sadanandhan, A. M., & Jain, S. L. (2019). Silver doped reduced graphene oxide as a promising plasmonic photocatalyst for oxidative coupling of benzylamines under visible light irradiation. New Journal of Chemistry, *43*(23), 9116–9122, doi:https://doi.org/10.1039/C9NJ00852G.
30. Ashok, A., Kumar, A., Matin, M. A., & Tarlochan, F. (2018). Synthesis of Highly Efficient Bifunctional Ag/Co_3O_4 Catalyst for Oxygen Reduction and Oxygen Evolution Reactions in Alkaline Medium. ACS Omega, *3*(7), 7745–7756, doi:https://doi.org/10.1021/acsomega.8b00799.
31. Chen, H., Xue, C., Cui, D., Liu, M., Chen, Y., Li, Y., et al. (2020). Co_3O_4–Ag photocatalysts for the efficient degradation of methyl orange. RSC Advances, *10*(26), 15245–15251, doi:https://doi.org/10.1039/C9RA10437B.
32. Pervaiz, E., Syam Azhar Virk, M., Bingxue, Z., Yin, C., & Yang, M. (2017). Nitrogen doped RGO–Co_3O_4 nanograin cookies: highly porous and robust catalyst for removing nitrophenol from waste water. Nanotechnology, *28*(38), 385703, doi:https://doi.org/10.1088/1361-6528/aa8297.
33. Huang, T., Liu, X., Wang, M., Huang, H., & Huang, P. (2023). Co_3O_4 Supported on Graphene-like Carbon by One-Step Calcination of Cobalt Phthalocyanine for Efficient Oxygen Reduction Reaction under Alkaline Medium. Nanomaterials, *13*(7), 1241, doi:https://doi.org/10.3390/nano13071241.
34. Chen, Z., Gao, Y., Chen, X., Xing, B., Zhang, C., Wang, S., et al. (2019). Nanoarchitectured Co_3O_4/reduced graphene oxide as anode material for lithium-ion batteries with enhanced cycling stability. Ionics, *25*(12), 5779–5786, doi:https://doi.org/10.1007/s11581-019-03134-x.
35. Su, D., Xie, X., Munroe, P., Dou, S., & Wang, G. (2014). Mesoporous hexagonal Co_3O_4 for high performance lithium ion batteries. Scientific Reports, *4*(1), 6519, doi:https://doi.org/10.1038/srep06519.
36. Alshatwi, A. A., Periasamy, V. S., & Athinarayanan, J. (2014). Cytotoxic Effects of Engineered Nanoparticles in Human Mesenchymal Stem Cells. World Academy of Science, Engineering and Technology, *September 3*, 9999422, doi:https://doi.org/10.5281/zenodo.1096129.
37. Arsalan, N., Hassan Kashi, E., Hasan, A., Edalat Doost, M., Rasti, B., Ahamad Paray, B., et al. (2020). Exploring the Interaction of Cobalt Oxide Nanoparticles with Albumin, Leukemia Cancer Cells and Pathogenic Bacteria by Multispectroscopic, Docking, Cellular and Antibacterial Approaches. International Journal of Nanomedicine, *15*, 4607–4623, doi:https://doi.org/10.2147/IJN.S257711.
38. Chattopadhyay, S., Dash, S. K., Tripathy, S., Das, B., Kar Mahapatra, S., Pramanik, P., et al. (2015). Cobalt oxide nanoparticles induced oxidative stress linked to activation of TNF-α/caspase-8/p38-MAPK signaling in human leukemia cells. Journal of Applied Toxicology, *35*(6), 603–613, doi:https://doi.org/10.1002/jat.3080.
39. Chattopadhyay, S., Dash, S. K., Tripathy, S., Das, B., Mandal, D., Pramanik, P., et al. (2015). Toxicity of cobalt oxide nanoparticles to normal cells; an in vitro and in vivo study. Chemico-Biological Interactions, *226*, 58–71, doi:https://doi.org/10.1016/j.cbi.2014.11.016.
40. Faisal, M., Saquib, Q., Alatar, A. A., Al-Khedhairy, A. A., Ahmed, M., Ansari, S. M., et al. (2016). Cobalt oxide nanoparticles aggravate DNA damage and cell death in eggplant via mitochondrial swelling and NO signaling pathway. Biological Research, *49*(1), 20, doi:https://doi.org/10.1186/s40659-016-0080-9.
41. Goudarzi, M., & Salavati-Niasari, M. (2019). Synthesis, characterization and evaluation of Co_3O_4 nanoparticles toxicological effect; synthesized by cochineal dye via environment friendly approach. Journal of Alloys and Compounds, *784*, 676–685, doi:https://doi.org/10.1016/j.jallcom.2019.01.028.
42. Lugun, O., Singh, J., Thakur, R. S., & Pandey, A. K. (2022). Cobalt oxide (Co_3O_4) nanoparticles induced genotoxicity in Chinese hamster lung fibroblast (V79) cells through modulation of

reactive oxygen species. Mutagenesis, *37*(1), 44–59, doi:https://doi.org/10.1093/mutage/geac005.

43. Papis, E., Rossi, F., Raspanti, M., Dalle-Donne, I., Colombo, G., Milzani, A., et al. (2009). Engineered cobalt oxide nanoparticles readily enter cells. Toxicology Letters, *189*(3), 253–259, doi:https://doi.org/10.1016/j.toxlet.2009.06.851.
44. Wahab, R., Siddiqui, M. A., Ahmad, J., Saquib, Q., & Al-Khedhairy, A. A. (2021). Cytotoxic and molecular assessment against breast (MCF-7) cancer cells with cobalt oxide nanoballs. Journal of King Saud University - Science, *33*(5), 101467, doi:https://doi.org/10.1016/j.jksus.2021.101467.
45. Wang, H., Ren, T., Zhu, N., Yu, Q., & Li, M. (2018). Co_3O_4 nanoparticles at sublethal concentrations inhibit cell growth by impairing mitochondrial function. Biochemical and Biophysical Research Communications, *505*(3), 775–780, doi:https://doi.org/10.1016/j.bbrc.2018.10.002.
46. Famuyide, I. M., Aro, A. O., Fasina, F. O., Eloff, J. N., & McGaw, L. J. (2019). Antibacterial and antibiofilm activity of acetone leaf extracts of nine under-investigated south African Eugenia and Syzygium (Myrtaceae) species and their selectivity indices. BMC Complementary and Alternative Medicine, *19*(1), 141, doi:https://doi.org/10.1186/s12906-019-2547-z.
47. Hughes, T. B., Dang, N. L., Miller, G. P., & Swamidass, S. J. (2016). Modeling Reactivity to Biological Macromolecules with a Deep Multitask Network. ACS Central Science, *2*(8), 529–537, doi:https://doi.org/10.1021/acscentsci.6b00162.
48. Bailly, C. (1998). Sequence-specific DNA minor groove binders. Design and synthesis of netropsin and distamycin analogues. Biocon Chem, *9*, 513–538.
49. Dolenc, J., Borštnik, U., Hodošček, M., Koller, J., & Janežič, D. (2005). An ab initio QM/MM study of the conformational stability of complexes formed by netropsin and DNA. The importance of van der Waals interactions and hydrogen bonding. Journal of Molecular Structure: THEOCHEM, *718*(1), 77–85, doi:https://doi.org/10.1016/j.theochem.2004.12.019.